Density Functional Theory Modeling and Calculation of NMR Parameters: An ab Initio Study of the Polymorphs of Bulk Glycine

ARTICLE *in* CRYSTAL GROWTH & DESIGN · JULY 2010

Impact Factor: 4.89 · DOI: 10.1021/cg100525h · Source: OAI

7 AUTHORS, INCLUDING:

Lorenzo Stievano
Université de Montpellier, Montpellier, France
131 PUBLICATIONS **1,643** CITATIONS
SEE PROFILE

Frederik Tielens
Collège de France
93 PUBLICATIONS **1,314** CITATIONS
SEE PROFILE

Dominique Costa
MINES ParisTech
94 PUBLICATIONS **1,744** CITATIONS
SEE PROFILE

Jean-François Lambert
Pierre and Marie Curie University - Paris 6
151 PUBLICATIONS **2,634** CITATIONS
SEE PROFILE

DOI: 10.1021/cg100525h

CRYSTAL GROWTH & DESIGN Article

2010, Vol. 10 3657–3667

Density Functional Theory Modeling and Calculation of NMR Parameters: An ab Initio Study of the Polymorphs of Bulk Glycine

Lorenzo Stievano,[†,‡,⊥] Frederik Tielens,[†,‡] Irène Lopes,[†,‡] Nicolas Folliet,[†,‡,§,#] Christel Gervais,[§,#] Dominique Costa,[∥] and Jean-François Lambert*[,†,‡]

[†]*UPMC Université Paris 06, UMR 7197, Laboratoire de Réactivité de Surface, Tour 54-55, 2ème étage - Casier 178, 4 Place Jussieu, F-75252 Paris CEDEX 05, France,* [‡]*CNRS, UMR 7197, Laboratoire de Réactivité de Surface, Tour 54-55, 2ème étage - Casier 178, 4, Place Jussieu, F-75252 Paris CEDEX 05, France,* [§]*UPMC Université Paris 06, Laboratoire de Chimie de la Matière Condensée de Paris, UMR 7574, Collège de France, 11 place M. Berthelot, 75005 Paris, France,* [#]*CNRS, UMR 7574, Laboratoire de Chimie de la Matière Condensée de Paris, Collège de France, 11 place M. Berthelot, 75005 Paris, France, and* [∥]*Ecole Nationale Supérieure de Chimie de Paris, Laboratoire de Physico-Chimie des Surfaces, 11 rue Pierre et Marie Curie, F-75231 Paris cedex, France.*
[⊥]*Current address: ICGm-AIME - UMR 5253, Case Courrier 1502, Université Montpellier II, 2 Place Eugène Bataillon 34095 Montpellier cedex 5, France.*

Received April 20, 2010; Revised Manuscript Received June 26, 2010

ABSTRACT: The three forms of glycine in the solid state, α, *β*, and *γ*, are described and modeled by means of generalized-gradient approximation (GGA) ab initio calculations. In particular, the location of the protons in each structure is studied. The vibrational frequencies and the NMR chemical shifts of ^{1}H, ^{13}C, and ^{15}N in the three polymorphs are calculated and compared to experimental data (IR and Raman, solid-state magic angle spinning NMR, respectively). ^{13}C chemical shift differences on the order of 1 ppm, which constitute the most accurate way to discriminate between the three structures when X-ray diffraction is not available, can be satisfactorily predicted.

Introduction

Glycine, the smallest amino acid, is a very interesting molecule with a relatively complex chemistry in the solid state. In fact, several polymorphs of crystalline glycine are known, all of them characterized by the presence of the glycine molecules in the zwitterionic state, that is, with a deprotonated carboxylate and a protonated ammonium function, organized in the solid state by specific networks of hydrogen bonds.[1]

Since the early work of Bernal, three main polymorphs are known to exist at ambient conditions, namely α-, *β*-, and *γ*-glycine.[2] These different solid state forms (vide infra) are very useful as biomimetic reference compounds: first of all, even though no peptide bonds are present, their molecular organization have structural similarities with the secondary structure of amino acids in glycine polypeptides: planar arrangements exist in the α- and *β*-forms (similar to the *β*-sheets of peptides) and helicoidal arrangements in the *γ*-form (similar to the α-helices of peptides).[3−5] Moreover, the continuous chains of zwitterions linked by NH---O hydrogen bonds existing in all these different structures are rather stable (for instance, they are preserved even during the polymorphic transformations) and can thus be considered to mimic peptide chains in biopolymers.[6] From a dynamic perspective, the study of the correlation between molecular and crystal structure of simple amino acids on the one hand, and lattice dynamics and phase transitions on the other hand, can be used to model systems for the study of conformational transitions and rearrangements of proteins.[7−10]

In addition to biomimetics, the study of polymorphism of small biological molecules is an important concern in solid-state chemistry and crystal growth technology; technologically relevant properties, such as the ease of dissolution and therefore the bioavailability, depend on the polymorphic state of the substance.[11] Various factors may be responsible for the formation of a specific amino acid polymorph during the complex processes occurring upon crystal growth, such as the existence of structured clusters in solution prior to crystallization, the structure of crystal surfaces that constitute nuclei for crystal growth, the interaction between these surfaces and the solvent, the presence of impurities in the preparation solution, and solvent−solute and solute−solute interactions.[12] The conditions of formation of different polymorphs of apparently simple systems, such as glycine, have been studied extensively in order to understand the influence of these factors, and of possible additives, in the precipitation of a specific polymorph from solutions of different compositions.[13−18]

In the following article, we will first summarize the structural differences between the three best-known crystalline forms of glycine, underlining the existence of an intermediate level of organization consisting of supramolecular units (sheets, layers, or helices) and then evaluate the results of a periodic density function theory (DFT) modeling of these polymorphs using several successive levels of optimization, by systematically comparing DFT predictions with experimental data on energetics, vibrational spectroscopy, and solid-state ^{1}H, ^{13}C, and ^{15}N NMR.

Description of the Glycine Polymorphs. After they were identified by Bernal, the structures of α-, *β*-, and *γ*-glycine were first precisely determined by single-crystal diffraction by Kvick and Iitaka[19−21] and successively refined several times (other polymorphs exist but can only be obtained in conditions very remote from standard ones). For α- and *γ*-glycine, single-crystal neutron diffraction

*Corresponding author. E-mail: jean-francois.lambert@upmc.fr.

Published on Web 07/15/2010

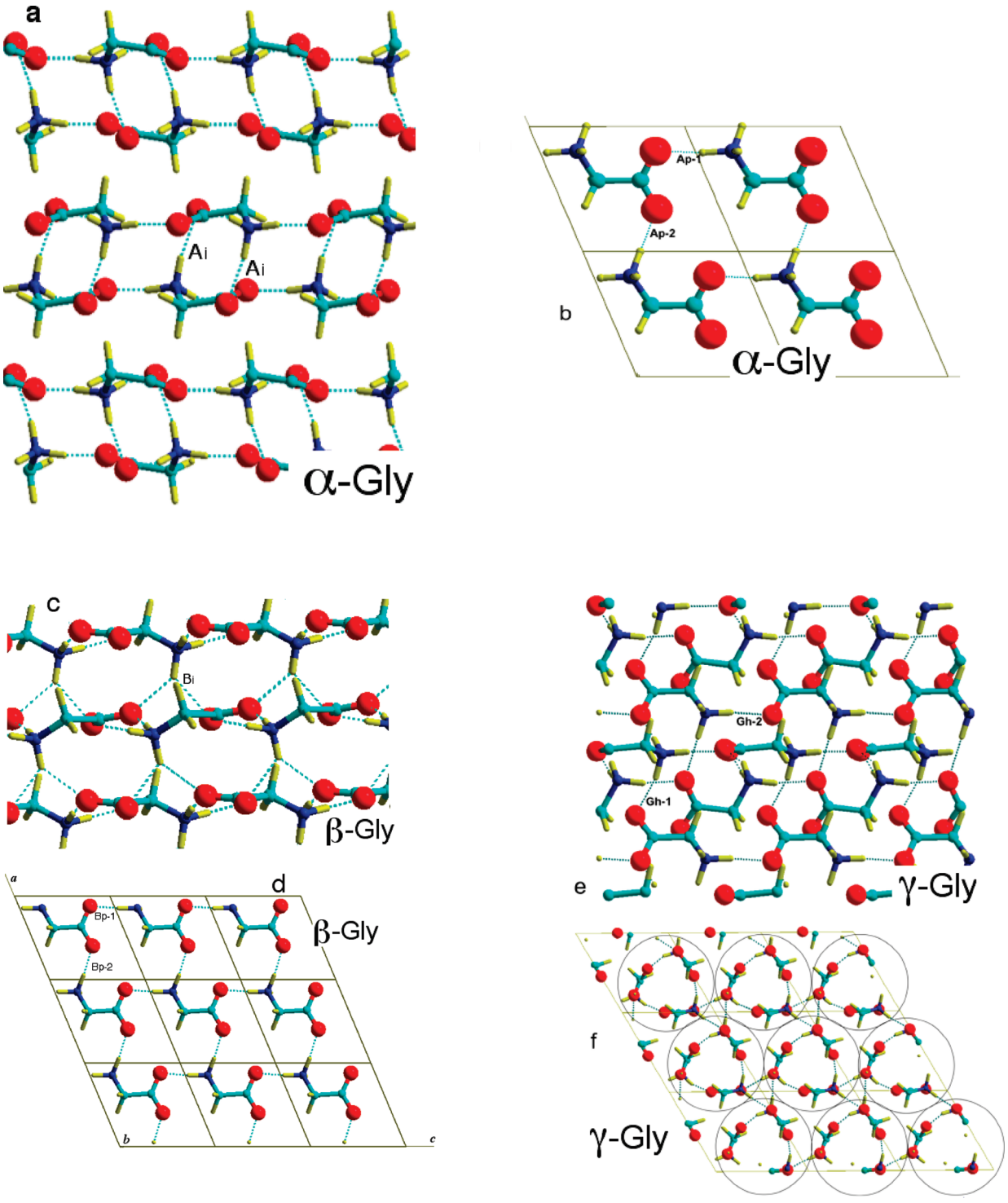

Figure 1. (a) Neighboring glycine molecules in three successive layers in the structure α-glycine; note the internal structure of the layers, consisting in two H-bonded planar sheets. (b) Single layer of glycine molecules in the α structure, viewed perpendicular to the *b* crystal axis. (c) Stacking of three layers of glycine molecules along the *b* axis in *β*-glycine. (d) Single layer of glycine molecules in the b structure; notice near equivalence to b. (e) Helicoidal arrangement of glycine molecules along the *c* axis in *γ*-glycine. (f) Honeycomb arrangement of the glycine helices in the *ac* planes of *γ*-glycine.

studies[22,23] also provided reliable information on the position of the hydrogen atoms. In the case of *β*-glycine, however, only single-crystal X-ray diffraction analyses are available to the best of our knowledge,[24] and therefore the position of the hydrogen atoms can only be estimated by calculation.

In each structure, all glycine molecules are crystallographically equivalent; they form significantly different supramolecular arrangements, sheets and layers in the case of α- and *β*-glycine, helices for *γ*-glycine.

α-Glycine (monoclinic, space group $P2_1/n$ (14)) consists of the stacking of consecutive layers along the *b* crystal axis. Each layer is formed by two ordered sheets of glycine molecules (Figure 1a,b) lying opposite to each other, so that two neighboring glycine molecules are ordered in a head-to-tail

arrangement, forming distinct dimeric adducts of glycine molecules (Figure 1a). Successive layers only interact through van der Waals-type interactions, while the integrity of each layer is ensured by a specific lattice of H bonds. This strong anisotropy of chemical bonding is an interesting feature that could be compared with more familiar layered materials such as clay minerals.

It will be important to distinguish the different hydrogen bonds that exist in this lattice, and we will use the following nomenclature:

(a) Hydrogen bonds between glycine molecules in a single sheet will be denoted as Ap (where A stands for "Alpha-glycine", and p for "planar"). There are two types of in-plane hydrogen-bonds, denoted Ap-1 and Ap-2 (Figure 1b). Both are almost linear N−H···O bonds; each glycine zwitterion is globally involved in four in-plane bonds, two as a donor and two as an acceptor.

(b) Intersheet hydrogen bonds, between two molecules in adjacent sheets. Each molecule of glycine is involved in two intersheet bonds, one as a donor and one as an acceptor. They are denoted as Ai (where i stands for "intersheet", see Figure 1a).

No close hydrogen contacts are formed between successive layers of α-glycine; it should be mentioned however that one C−H of the methylene group points out toward the neighboring layer, more precisely between two oxygen atoms at a distance of about 2.3 Å. This would result at best in weak hydrogen bonding.

In β-glycine (monoclinic, space group $P2_1$ (4)), the glycine molecules are also ordered in bidimensional sheets with alternate orientation of the molecules between two successive sheets. In this case, however, two successive sheets are slightly translated so that they do not form an identifiable layer. The arrangement of the glycine molecule within a single sheet is almost identical to that of α-glycine; that is, two types of in-plane hydrogen bonds are formed, along the *c* axis and along the *a* axis (cf. Figure 1c); we will denote them respectively as Bp-1 and Bp-2, using a nomenclature similar to that of α-glycine.

There are intersheet H-bonds in this case too, and they will be denoted respectively as Bi-1 and Bi-2 (Figure 1d). These are bifurcated H-bonds, where the donor is a single N−H group, while the acceptors are two oxygen atoms belonging to the carboxylic groups of two different glycine zwitterions in the neighboring sheet. It should be underlined that each sheet is equally H-bonded to its two neighboring sheets in the stacking, while in α-glycine, H-bonding is only to one side of a given sheet, thus forming layers of two sheets as well-identifiable hierarchical units.

The structure of γ-glycine (hexagonal, space group $P3_2$ (145)) is completely different from those of the other two polymorphs. In this structure, glycine molecules form helicoidal arrangements along the *c* axis (Figure 1d). The identifiable supramolecular units are these helices, instead of planar arrangements (sheets and layers) as in the other two polymorphs. Two different hydrogen-bonds are formed, denoted as Gh-1 and Gh-2 (where h of course stands for "helicoidal"). These helices are then further ordered in a hexagonal honeycomb arrangement, as depicted in Figure 1e, with the establishment of one additional H-bond, named Gi. In such an arrangement, each glycine molecule takes part in six H-bonds to other glycine molecules, four in the helicoidal stacking and two to other helices in the honeycomb arrangement.

In standard conditions, γ-glycine is the thermodynamically most stable polymorph.[25] However, this form can only be precipitated from either acidic or basic solutions, whereas α-glycine usually precipitates from supersaturated neutral aqueous solutions.[20,26] α-Glycine, while metastable in principle, only transforms to the more stable γ-form when exposed to humid NH_3.[25,27] β-glycine, usually precipitated either from an ethanol−water mixture or from acetic acid solutions, is the least stable polymorph and rather quickly transforms to α-glycine unless stored under strictly dry conditions.[9,24,28]

Since the initial work of Almlöf et al.,[29] several theoretical studies have addressed the stability of the different polymorphs of glycine. Already in 1998, Freeman et al.[30] studied the relative stability of the three polymorphs of glycine by periodic DFT employing BLYP functionals, and found a very good agreement between experimental and calculated structures. Only very minor differences in energy (of the order of about 3.5 kJ/mol, i.e., 0.037 eV) between the different forms were obtained, α-glycine being the most stable one. These differences were considered too small to be significant, especially considering that vibrational entropy was not included in this calculation of the free energies. Similar results were also found by Raabe by MINDO/3 semiempirical methods.[31]

A more complete study on the relative stability of α-, β-, and γ-glycine is presented in the work of Chisholm et al.,[32] who studied in addition high-pressure and even hypothetical polymorphs of this amino acid. In this work, the efficiency of different functionals (LDA, PW91, and PBE) in the determination of the relative stability of the polymorphs was evaluated. The authors found that while LDA (local density approximation) functionals tend to overestimate the strength of hydrogen bonds, leading to cell lattices more compact than the experimental ones by about 10%, generalized gradient approximation (GGA) functionals such as PW91 or PBE overestimate covalent bond lengths,[33] leading to 5−10% too low densities for the glycine crystals. More recently, Chowdry et al[34] confirmed that bond lengths in solid glycine calculated with PW91 and PBE are too long, whereas H bond lengths are too short, with a net effect leading to increased cell parameters as compared to the experimental ones.

The energy differences between the three stable polymorphs were found to be even smaller than those from the work of Freeman et al.;[30] for instance, using PBE functionals, differences of less than 0.85 kJ/mol were obtained between the three forms of glycine, α-glycine being found once again as the most stable polymorph. In summary, the authors confirmed the difficulty in predicting the relative stability of the three polymorphs due to the very small energy differences.

Recently, more advanced methods including a specific treatment of the intermolecular interactions, such as the inclusion of an electrostatic multipole description of the interacting molecules,[35] or the inclusion of vibrational zero-point energy contribution,[36] were applied to the problem. In these cases, a more accurate prediction of the relative stability of the glycine polymorphs was attained.

Thus, it appears that the study of glycine polymorphism is an interesting test for the accuracy of molecular modeling techniques. Since this problem involves very small energy differences, additional experimental tests of modeling results

would be helpful. In the following sections, we will show that NMR spectroscopic parameters can play such a role (in addition to the more often used vibrational spectroscopy) since they are sensitive to the different patterns of hydrogen bonds.

Glycine is indeed a very interesting molecule from the point of view of NMR spectroscopy, since all of its atoms have isotopes amenable to an NMR study, namely, ^{1}H ^{13}C, ^{14}N, ^{15}N, and ^{17}O. Among these, ^{14}N and ^{17}O are quadrupolar while ^{1}H, ^{13}C, and ^{15}N are spin 1/2 nuclei whose study is rather straightforward.

In a previous study, our group has shown that the GIPAW method can provide reliable predictions for the chemical shifts of different amino acids.[37] In the present work we wish to demonstrate that the precision of this calculation method allows an extension to different polymorphs of the same amino acid, within very narrow ranges of chemical shifts.

Materials and Methods

Synthesis of the Glycine Polymorphs. α-Glycine was obtained commercially (Sigma, purity >99%) and used without further purification. Appropriate aqueous solutions of the same commercial α-glycine were also used for the synthesis of the other two polymorphs. *β*-Glycine was synthesized using the antisolvent method of Iitaka, by adding ethyl alcohol to a concentrated aqueous solution of glycine.[19] *γ*-Glycine was obtained by cooling a saturated solution of glycine and acetic acid.[24] The purity of the different polymorphs was checked by X-ray diffraction before the spectroscopic measurements. X-ray powder diffractograms (not shown) were recorded on a Siemens D5000 diffractometer using CuK_α radiation (λ = 154.05 pm).

Fourier Transform Infrared (FT-IR) and Raman Spectroscopies. FT-IR spectra of the pure compounds were recorded in the attenuated total reflection (ATR) mode on the pure compounds with a Thermo Nicolet FT-IR spectrometer. This is preferable to working in the transmission mode on self-supported films or KBr pellets, since high pressures have been reported to influence the position of the infrared and Raman bands significantly.[38]

Raman spectra were collected at room temperature with a Kaiser Optical Systems HL5R Raman spectrometer equipped with a near-IR laser diode working at 785 nm. The laser power was adjusted to 10−15 mW at the sample position for all spectra, and the resolution was 3 cm^{-1}.

The obtained FT-IR and Raman spectra are virtually identical to those obtained in previous studies of glycine polymorphs under the same conditions.[38−42]

NMR Spectroscopy. The ^{1}H experiments were recorded on Bruker Avance III 500 (magnetic field 11.8 T) and 700 (16.5 T) spectrometers. At 11.8 T, a 4 mm double resonance magic angle spinning (MAS) probe was used, spinning at 10 kHz while at 16.5 T, an ultrafast MAS 1.3 mm double resonance probe spinning at 67 kHz was used. ^{1}H chemical shifts are referenced to external TMS.

w-DUMBO Experiments at 11.8 T. The wDUMBO shape consists of a phase-modulated function. We have employed a shape composed by one cycle of 64 steps.[43] The pulse length for the DUMBO shape was set to 24 μs for a 100 kHz decoupling strength. The detection window t_w was set to 3.2 μs. RD = 3 s, NS = 32, $t_{\pi/2}(^{1}H)$ = 2.5 μs.

Solid-state ^{13}C and ^{15}N MAS NMR spectra were recorded at room temperature with a Bruker Avance 400 spectrometer at 9.4 T, equipped with a 4 mm probe and with variable spinning rates. ^{13}C spectra were obtained using a proton cross-polarization with a 90° pulse length of approximately 3 μs, a contact time of 1 ms, a data acquisition time of 154 ms, and a recycle delay of 5−10 s. The chemical shifts were determined by reference to an external adamantane sample (38.52 ppm). As we mentioned elsewhere,[44] the contact time is an important parameter if one wants to quantify the signals of different glycine forms, but in the present paper we only discuss the chemical shifts of pure phases.

^{15}N spectra were obtained using a proton cross-polarization with a 90° pulse length of 5 μs, a contact time of 5 ms, a data acquisition time of 44 ms, and a recycle delay of 5 s. The chemical shift were determined using α-glycine itself as a secondary reference (−346.6 ppm).

Computational Methodology. All calculations are performed using ab initio plane-wave pseudopotential periodic DFT as implemented in VASP.[45] The revised Perdew−Burke−Ernzerhof (rPBE) functional[46] has been chosen to perform the periodic DFT calculations. The accuracy of the method has been tested elsewhere.[47] Pure GGAs are known to underestimate bonds and overestimate H bonds.[33,48] It is also known that DFT methods in general (pure or hybrid) fail to describe medium and long-range forces.[49−52] For example, pure and hybrid GGAs fail to describe the improved stability of the glycine dimer stacked structure, as compared to the cyclic planar geometry.[53,54] However, the pure functionals PW91 and PBE have been shown[55] to correctly describe medium range forces for a number of molecules as rare gas dimers,[55,56] methane, ethene, and benzene dimers,[55] hydrogen-bonded systems,[55] amide dimers,[57] amino acids in the solid state,[58] crystalline urea[59] and DNA bases.[60,61] Finally, dispersion forces are lacking in DFT approaches.

The valence electrons are treated explicitly and their interactions with the ionic cores are described by the projector augmented-wave (PAW) method[62,63] which allows the use of a low energy cutoff for the plane-wave basis. The cutoff used in the calculations is set equal to 400 eV.

A (5 × 5 × 5) *k*-point grid is used in the Brillouin-zone sums, and the partial occupancies are set for each wave function using the tetrahedron method with Blöchl corrections.[62] The convergence is checked with the number of *k*-points. The positions of all the atoms in the supercell are relaxed, in the potential energy determined by the full quantum mechanical electronic structure until the total energy differences between the loops is less than 10^{-4} eV. The structure of the glycine polymorphs has been optimized in three successive steps, starting from the published neutron diffraction (available for α- and *γ*-glycine) or the X-ray diffraction structures (in the case of *β*-glycine, where the H atoms were initially located based on reasonable guesses). In the first step, only the position of the hydrogen atoms was relaxed; in the second step, all atomic positions were allowed to relax while the lattice parameters were frozen; and in the third step, all lattice parameters as well as all atomic positions were left free.

We refer as "stabilization" energy to the cohesion energy of each solid phase, calculated as $E_{stab} = E(\text{solid phase})/n - E(\text{gaseous Gly})$, where E(solid phase) is the total energy of the unit cell of the α, *β*, or *γ* phase, n is the number of glycine molecules in the unit cell, and E(gaseous Gly) is the total energy of one neutral glycine molecule in a box large enough so that the molecule is considered isolated in the gas phase.[64,65]

In some cases, the stabilization energy in one layer was calculated. The glycine layer was separated from the next layers by vacuum, and after performing a single point calculation, the same formula $E_{stab} = E(\text{glycine layer})/n - E(\text{gaseous Gly})$ was applied.

To calculate the Hessian matrix, finite differences are used; that is, each ion is displaced in the direction of each Cartesian coordinate, and the Hessian matrix is determined from the forces. All atoms are displaced in all three Cartesian directions. The frequency calculations are performed considering only the Gamma point.

The NMR parameters were calculated within Kohn−Sham DFT using the QUANTUM-ESPRESSO code[66,67] in which the GIPAW method[68] was implemented, keeping the atomic positions and cell constants equal to the values previously calculated with VASP. Details about the computation of the isotropic chemical shifts for ^{1}H, ^{13}C, and ^{15}N are reported elsewhere.[37,69]

Results and Discussion

1. Geometry and Covalent Bonds. The calculated geometrical parameters are compared to the experimental ones obtained by diffraction techniques in Table 1. Only small modifications of the cell parameters (≤5 pm) are observed for the three forms of glycine. All parameters decrease: thus, we observe the effect reported by Chowdhry et al.[34] and attributed to the well-known tendency of GGA functionals to overestimate covalent bond lengths is offset by the equally

Table 1. Comparison of Experimental and Calculated Unit Cell Parameters

structure	parameter	diffraction data	cell and atomic position opt	Δ [%]
α-glycine[a]	*a* [Å]	5.102	5.102	0.0
	b [Å]	11.971	11.828	−1.2
	c [Å]	5.458	5.435	−0.4
	β [deg]	111.71	111.84	0.1
	vol [Å^3]	309.69	304.43	−1.7
β-glycine[b]	*a* [Å]	5.092	5.080	−0.2
	b [Å]	6.273	6.208	−1.0
	c [Å]	5.384	5.355	−0.5
	β [°]	113.17	113.37	0.2
	vol [Å^3]	158.10	155.03	−1.9
γ-glycine[c]	*a*, *b* [Å]	7.046	6.963	−1.2
	c [Å]	5.491	5.453	−0.7
	α [°]	120	120	0.0
	vol [Å^3]	230.59	228.90	−0.7

[a] Monoclinic, space group $P2_1/n$ (14), cf. ref 22. [b] Monoclinic, space group $P2_1$ (4), cf. ref 24. [c] Trigonal, space group $P3_2$ (14), cf. ref 23.

well-known tendency to underestimate H-bond lengths. It is interesting to notice however that the calculation method we used (rPBE/planewaves) gives cell parameters and volumes closer to the experimental values, as compared to previous computational studies.[32]

We shall now consider the effect of structure optimization on local features, starting with the internal geometry of groups involved in H-bonding, that is, the N−H and C−H covalent bonds. For α-glycine, in particular, geometry optimization modifies the C−H and N−H bond lengths. The two C−H bonds of the methylene group have about the same length (they differ by at most 0.7 pm, either in the experimental data or in successive optimizations). In contrast, the different N−H bonds are not exactly equivalent because they are involved in different patterns of H bonding: the difference between the extreme values for N−H lengths is between 2.4 and 3.3 pm. The hydrogen involved in the formation of the "head-to-tail" glycine dimer (Ai type H-bond) always remains closer to the nitrogen atom.

In the case of α-glycine, while the neutron diffraction structure indicates two relatively short and one longer N−H covalent bond, the optimization of the position of the hydrogen atoms leads to two relatively long and one short N−H distance. The two longer distances correspond to the atoms involved in the H-bond network in the *ac* plane (Ap-1 and Ap-2, see § 2), where the hydrogen is displaced toward the H-bond acceptor.

For *β*-glycine where no neutron diffraction results were available, the initial estimates of hydrogen positions (based on the positions of the other atoms as evaluated by X-ray diffraction) seem to provide too short N−H distances, and indeed the geometry optimization results in large variations of this parameter. The bond lengths after optimization are similar to those found for α-glycine: here too, the two longest H−N distances correspond to the atoms involved in intrasheet H-bonds (i.e., in the *ac* plane, Bp-1 and Bp-2). In contrast, the third hydrogen atom, forming two long hydrogen contacts with other molecules, remains closer to the nitrogen center.

In the case of *γ*-glycine, after optimization, the two longer N−H distances correspond to the groups involved in bonds stabilizing the supramolecular unit, which is in this case the helicoidal arrangement of glycine molecules.

Regarding the C−H bond lengths, in the case of α- and *γ*-glycine, the optimization steps have very little effect on the C−H bonds: between 1 and 2 pm. For *β*-glycine, the optimization results in a strong adjustment of C−H bond lengths.

Table 2. Comparison between Experimental and Calculated Structural Data—H-bond Lengths[a]

	H-bond type	neutron diffraction structure (α and *γ* Gly), or estimated from XRD data (*β* Gly)	atoms + cell relaxation
α-Gly	Ap-1	1.725	1.657
	Ap-2	1.827	1.764
	Ai	2.118	2.060
β-Gly	Bp-1	1.831	1.631
	Bp-2	2.028	1.779
	Bi	2.235	2.093
γ-Gly	Gh-1	1.812	1.761
	Gh-2	1.757	1.709
	Gi	1.940	1.910

[a] Values in Å.

Table 3

structure	Δ*E* (eV)	thermal contribution at 298 K (eV/cell)	ΔΔ*G* (eV/cell)
α-gly	0.01	2.08	0.00
β-gly	0.00	2.14	0.05
γ-gly	0.05	2.12	0.08

2. Hydrogen-Bonding. The hydrogen bonding patterns that define the crystal structure of glycine are strongly dependent on the calculation steps. Successive optimizations tend to decrease the (N−H)···acceptor distances, hereafter referred to as "H-bond lengths". The H-bonds internal to the supramolecular units (sheets or helices) remain significantly shorter than those between different units. The various H-bond lengths are reported in Table 2.

For α-glycine, upon relaxation, the three types of H bonds are shortened by the same order, 96, 96 and 97% for the Ap-1, Ap-2 and Ai, respectively, in comparison with experimental data.

For *β*-glycine, the starting atomic coordinates of the hydrogens were not exact, and the partial optimization (H positions only) indeed leads to a more realistic estimation of the hydrogen bonding parameters: in fact, the resulting hydrogen bond lengths are close to the values obtained for α-glycine. The complete relaxation of all atomic positions leads to a shortening of the H-bonds. As in the case of α-glycine, a more pronounced shortening is observed for the intersheet H-bonds as compared with intrasheet ones; the intersheet H-bonds of *β*-glycine evolve in a very similar manner to those of α-glycine as expected, while the intrasheet H-bonds behave differently, which is logical in view of the different stacking mode.

γ-Glycine exhibits the general trends of shorter H-bonds within the supramolecular unit, and of general shortening upon optimization.

3. Energetics. The stabilization energies per glycine molecule of the different polymorphs are reported in Table 3. The energies calculated for the different forms of glycine are all very similar, and the differences fall within the uncertainty of the calculation method, which can be estimated to a few hundredths of eV (i.e., a few kJ/mol). This conclusion agrees with previously published calculations,[25,34] which also found differences on the order of a few hundredths of eV among the three forms of glycine.[30,32] In our case, the differences are

Table 4. Experimental and Calculated Vibrational Spectra of α-, β-, and γ-Glycine (Calculated for Optimized Structures) in the 200−4000 cm^{-1} Range

	α-glycine						β-glycine				γ-glycine				
vibration	IR	Raman	calculated components				IR	Raman	calculated components		IR	Raman	calculated components		
$\delta_{as}(NH_3)$	(sh)	1665	1703	1701	1671	1670	(sh)	1655 (w)	1685	1660	1665	1670	1714	1712	1699.5
$\delta_{as}'(NH_3)$	1611	1628 (w)	1668	1665	1655	1650	1611		1657	1656	1629	1630	1662	1661	1645
$\nu_{as}(CO_2)$; $\delta_s(NH_3)$	1596	(1563?)	1603	1594	1591	1589	1594	(1560?)	1621.5	1599.5	1576	1575	1607	1597	1594
$\nu_{as}(CO_2)$; $\delta_s(NH_3)$	1525, 1505	1511 (sh), 1500	1543	1542	1536	1533	1525, 1503	1520	1553	1539	1499, 1481	1495	1529	1527	1503
$\delta(CH_2)$	1445	1451, 1434	1475	1472	1455	1452	1443	1443	1458	1453.5	1437	1435	1455	1450	1442
$\omega(CH_2)$; $\rho_{op}(NH_3)$	1413	1406	1402	1400	1399	1397	1413	1405	1398	1396	1391	1395 (br)	1398	1397	1392
$\omega(CH_2)$; $\rho_{op}(NH_3)$	1334	1320	1336	1335	1332	1331	1334	1317	1336	1323	1335	1332	1355	1354	1348.5
$\tau(CH_2)$;$\rho_{op}(NH_3)$	1312	(1308) sh	1329	1327	1325	1322.5	(1310) sh	1316	1320	1310	1324	1318	1338	1337	1335
$\nu(CN)$; $\omega(CH_2)$; $\rho_{ip}(NH_3)$	1133	1133	1172	1168	1168	1161	1131	1139	1160.5	1151	1154	1150	1187.5	1186.5	1169.5
$\tau(CH_2)$; $\rho_{op}(NH_3)$	1113	1104	1122	1122	1119	1117.5	1112	1100 (w)	1112	1101	1128	1128	1143	1141	1135
$\nu(CN)$	1034	1030	1056	1053	1053	1052	1034	1035	1047	1045	1043	1044	1069	1068	1066
$\rho(CH_2)$; $\omega(CO_2)$; $\rho_{op}(NH_3)$	911	916	925	922	913.5	912	911	911	900	898	930	925	928.5	924	919
$\nu(CC)$; $\delta(CO_2)$	893	888	895	895	894	893	893	888	885	884	889	888	892	888	888
$\delta(CO_2)$; $\delta(CCN)$	699	693	700	700	700	698.5	699	700	699	696	686	682	693	693	688
$\tau(CN)$		598	648	646	620	616		602	601	600		601	672	666	663
$\omega(CO_2)$		503	578	578	577	577		506	560	557		553	577	574	566
$\rho(CO_2)$		491	496	491	490	483		483	475	466		500	506	504	503
$\delta(CCN)$		354	385	383	375	374		342	366	363		355	386	385	375

even smaller: the lattice energies were found to be, in decreasing order, $\gamma > \alpha > \beta$, with the three forms all being in a range of 6 kJ/mol independent of the level of relaxation. The calculation of the frequencies (vide infra) has allowed us to estimate the thermal contributions (enthalpy and entropy) to the total energy. These contributions are reported in Table 3. Interestingly, the α phase is now the most stable structure, due to the larger number of degrees of freedom than the β and γ phase, as explained below (calculation of the vibrational spectra).

It is possible that the inclusion of dispersion forces would provide more accurate estimates of the relative stability of different polymorphic crystal structures: we have underlined above that an accurate estimate of the relative order of stability of the glycine polymers is a stringent test for DFT calculations, and it was not the main purpose of our investigation.

It is interesting to estimate how the total lattice energy is partitioned among the different hydrogen bonds present in the structure. The stabilization energy for the three forms is 1.7−1.8 eV, corresponding to about 170 kJ·mol^{-1}. If this additional stabilization energy is entirely attributed to H-bonds, this would correspond to an average of about −28 kJ/mol per H-bond in α- and γ-glycine where each molecule is involved in six H-bonds, and −21 kJ/mol per H-bond in β-glycine where each molecule is involved in eight H-bonds. These estimations correspond to rather strong H-bonds: for comparison, the H-bond strength in the water dimer has been calculated to 22.5 kJ/mol and that of the $(H_2O)(NH_3)$ complex of 29.5 kJ/mol, as compared to 19.7 for $(H_2O)_2$ and 25.01 for $(H_2O)(NH_3)$ respectively at the MP2 level.[33]

In the case of α-glycine, calculations made for sections of the partially optimized structure (calculation made with a single *k*-point and no further geometrical optimization) showed that the contribution of the intrasheet H-bonds stabilizing the glycine dimers (Ai H-bonds in Figure 1a) is about −0.65 eV (−62.7 kJ.mol^{-1}), whereas the contribution of the ordering in the *ac* plane (intersheet Ap-1 and Ap-2 H-bonds, cf. Figure 1b) is about −1.3 eV (−125.5 kJ·mol^{-1}). Thus, the dominant effect is the formation of the 2-D sheets, and the pairing of the sheets in a layer results in an energetic effect about half as important.

In the case of β-glycine, the contribution of the intrasheet ordering in the *ac* plane (Bp-1 and Bp-2 H-bonds) was found to be very similar to the one in α-glycine, contributing about −1.2 eV (−115.8 kJ·mol^{-1}). Here too, this contribution is dominant compared to the stabilization in the *b* direction of the lattice. This result correlates well with the H-bond lengths since the intersheet H-bonds in α- and β-glycine are longer than those lying in the sheets.

The dominant intrasheet stabilization for both α- and β-glycine is also interesting considering the low activation barrier for the transformation of β to α glycine, which occurs at relatively low temperatures (300 K) by a rearrangement of the glycine molecules in the *b* direction of the lattice, involving a sliding displacement of the sheets relative to their neighbors.[24,28]

4. Calculation of the Vibrational Spectra. On these fully geometrically optimized structures, the vibrational frequencies have been calculated, not only in order to obtain spectroscopic properties but also to confirm the stability of the geometry. All structures were checked to be minima in the potential energy surface.

The calculation of the vibrational spectra of the three forms of glycine generated 120 different vibrational modes for α-glycine, 60 modes for β-glycine and 90 modes for γ-glycine. Taking into account that for the three structures, each glycine molecule sits on a C_1 symmetry site providing 30 degrees of freedom, and discarding the three lattice translational degrees of freedom, which are also included in the calculated modes by VASP, these results would lead to 117, 57, and 87 vibrational modes for α-, β-, and γ-glycine, respectively. The full symmetry analysis of the vibrational spectrum of α-glycine has already been reported by Chowdhry et al.,[34] who defined 24 internal coordinates for the local symmetry of the glycine molecule. These produce 96 internal modes, one-half active in Raman and one-half in infrared spectroscopy, and 21 external lattice and librational modes. The total of 117 modes corresponds to the number of modes calculated by VASP.

A similar analysis can be performed also for the other two forms of glycine: for β-glycine, one expects 48 internal and 9 external (lattice and librational) modes, whereas for γ-glycine

72 internal modes are found, the remaining 15 vibrations being external modes. It is interesting to note that, for γ-glycine, the local symmetry conditions are similar to those found for polyglycine II: the local symmetry is C_3 and all vibrations, of symmetry A and E, are active both in infrared and Raman spectroscopy.[70] This leads to the data reported in Table 4 (not corrected for anharmonic contributions), which are listed together with the Raman and infrared bands measured at ambient temperature.

The vibrational spectra (both Raman and infrared) of glycine polymorphs have already been the subject of many investigations, and the attribution of the vibrations appearing in the infrared and Raman spectra for the three crystalline forms have been studied both from the experimental[38−42] and the theoretical[34,71−76] points of view. In conformity with previously published spectra, we found that several bands of γ-glycine have noticeably different from the other two polymorphs, allowing to identify γ-glycine by simple fingerprint comparison. The differences between α- and β-glycine are more subtle, with only small shifts in Raman bands between 300 and 1700 cm^{-1}.

In general, the spectral region below 1700 cm^{-1} (Figure 2) is the most interesting one for several reasons: first, it is the range where one finds the vibrational frequencies differing most among the three glycine structures. Second, out of this range the assignment of the vibrational bands is not straightforward: for instance, the large multicomponent band centered around 3000 cm^{-1} arises from the overlap of several different peaks, which are mostly due to overtones and combination bands, and it is therefore difficult to assign each band to a specific vibration without specific isotopic studies (with the exception of the band at the topmost frequency). Finally, at the lower frequencies the calculated data are less sensitive to different anharmonic contributions and can be directly compared to the experimental ones without correction. As shown by Table 4, in the 600−1700 cm^{-1} range, the differences between calculated and experimental frequencies are always lower than 3%. While this correspondence is quite good, the experimental differences between the band positions of the three polymorphs are usually of the same order of magnitude.

Band assignments are also indicated in Table 4. For α-glycine, they agree well with those of Chowdhry et al.[34]

As an additional caveat, one has to take into account the fact that calculations were carried out at 0 K while our measurements are made at room temperature, and it is known that these spectra are very sensitive to external conditions; for instance, changes in temperature of 200 K may lead to shifts on the order of 10 cm^{-1} and (in one specific case) up to 55 cm^{-1}.[38]

5. Calculation of NMR Parameters. First principles NMR calculations (using the GIPAW method for the VASP optimized bulk glycine geometries discussed above) are compared to the experimental values, which have been measured for ^1H, ^{13}C, and ^{15}N for the three structural forms of glycine (Table 5).

5.1. ^1H NMR. Well-resolved proton spectra are difficult to obtain due to strong homonuclear dipolar coupling. The resolution can be efficiently enhanced by combining rotation of the sample with the application of homonuclear decoupling sequences that average out the spin parts of the $^1H-^1H$ dipolar interactions. These are referred to as combined rotation and multiple-pulse spectroscopy (CRAMPS) techniques such as frequency switched Lee−Goldburg (FSLG),[77]

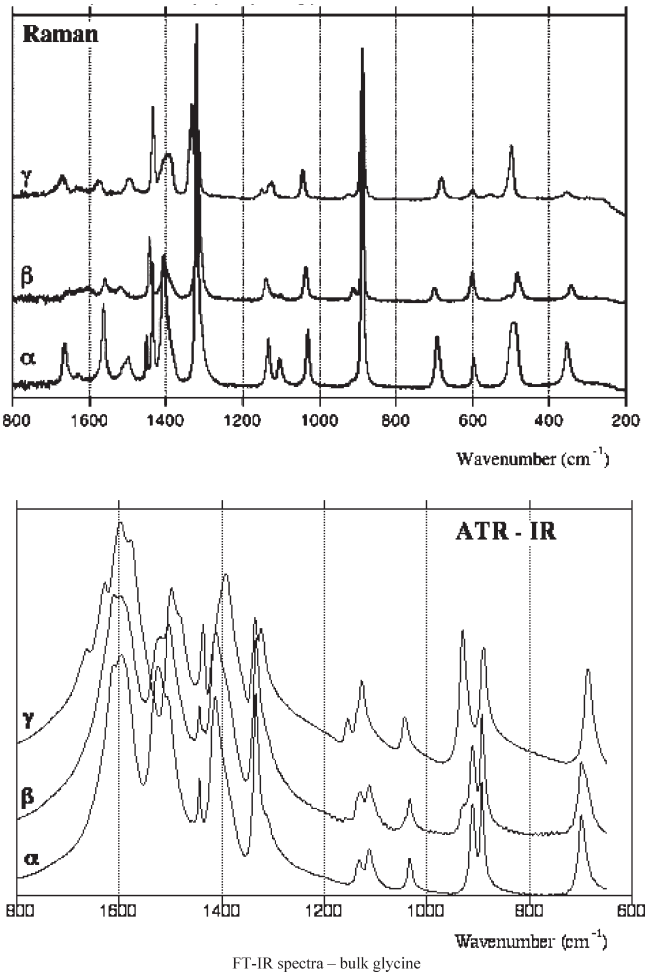

Figure 2. Experimental Raman (top) and ATR-IR (bottom) spectra of three polymorphs of glycine.

phase modulated Lee−Goldburg (PMLG)[78] and decoupling under mind boggling optimization (DUMBO).[79] These methods are very efficient but exhibit an inherent difficulty due to the scaling of the shielding tensor which is often experimentally slightly different from the theoretical ones. As a result, CRAMPS methods have been extensively tested on α-glycine, but the resulting published positions of the methylene and ammonium groups vary within 1 ppm.[80−83]

To deal with this probem, we decided to record the ^1H MAS NMR spectra of α- and γ-glycine at very high field (16.5 T) and very high spinning speed (67 kHz) with a simple single pulse experiment (Figure 3a,c). They are characterized by two groups of signals corresponding, at increasing chemical shifts, to the methylene and to the ammonium groups, respectively. In the case of β-glycine, this high spinning speed was not used because it was feared that the low stability of this compound would lead to its transformation in the rotor.[84] Therefore, a proton spectrum was recorded using the w-DUMBO sequence (Figure 3e), a 1D windowed pulse sequence[85] to directly obtain a high-resolution ^1H spectrum. A consistent experimental scaling factor of 0.43 was determined by recording the α- and γ-glycine spectra in the same conditions (Figure 3b,d) and comparing the data with the high field/spinning speed spectra.

In the case of α-glycine, the signals corresponding to the two hydrogens of the methylene group are well resolved, giving two peaks centered at 2.6 and 3.8 ppm, respectively,

Table 5. Calculated Chemical Shifts for ^{1}H, ^{13}C, ^{15}N, and ^{17}O (^{1}H, ^{13}C and ^{15}N exp. data: this work; ^{17}O data for γ-gly: ref 91)

	α-glycine			β-glycine		γ-glycine		
	calculated			calculated		calculated		
(ppm)	neutron data	optimized positions	observed	optimized positions	observed	neutron data	optimized positions	observed
$N\underline{H}_3$	9.9	11.0		11.3		9.8	10.6	
$N\underline{H}_3$	7.4	8.4		8.2		7.7	8.8	
$N\underline{H}_3$	4.8	5.0		5.2		6.6	7.3	
$N\underline{H}_3$av	7.37	8.13	8.0	8.23	8.0	8.03	8.90	8.9
$C\underline{H}_2$	3.1	3.4	3.8	2.4		1.8	2.1	
$C\underline{H}_2$	1.9	2.0	2.3	2.1		1.4	1.9	
$C\underline{H}_2$av				2.25	2.7	1.60	2.00	3.1
$\underline{C}$=O	175.4	181.6	176.4	180.5	175.3	170.8	179.9	174.5
$\underline{C}H_2$	39.6	40.9	43.7	40.2	43.3	36.0	39.4	42.3
$\underline{N}H_3$	−345.0	−342.4	−346.1	−340.4	−347.7	−347.8	−343.6	−346.1
C=$\underline{O}$	298.2	311.9	280	304.7		279.9	302.6	280
C=$\underline{O}$	282.8	299.6	272	302.1		277.2	299.9	272

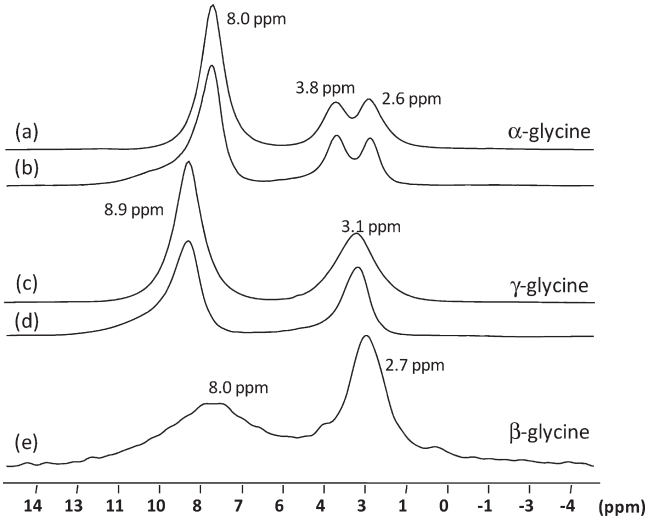

Figure 3. Experimental ^{1}H NMR spectra of α-glycine (a) MAS (67 kHz, 16.5 T), (b) w-DUMBO (10 kHz, 11.8 T), γ-glycine (c) MAS (67 kHz, 16.5 T) (d) w-DUMBO (10 kHz, 11.8 T), β-glycine, (e) w-DUMBO (10 kHz, 11.8 T).

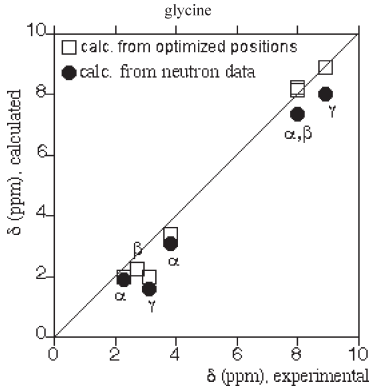

Figure 4. Comparison of calculated and experimental ^{1}H NMR isotropic chemical shifts for the methylene and ammonium groups in α-, β-, and γ-glycine.

whereas a single broad methylene signal is present in the case of β- and γ-glycine, centered at 2.7 ppm (β) and 3.1 ppm (γ). A single ammonium signal is observed for the three forms of glycine, centered at 8.0, 8.0, and 8.9 ppm, for α-, β-, and γ-glycine, respectively. The general structure of the ^{1}H CRAMPS NMR spectra published by Kimura et al.[83] for α- and γ-glycine, and Taylor et al. for α-glycine[86,87] (obtained at ω_L = 300 MHz) are similar although the reported chemical shifts are somewhat different.

For the three forms of glycine, the calculated chemical shifts change only very slightly at successive levels of cell optimization. The results of the calculations are summarized in Table 5.

The calculations lead to different chemical shifts for all protons in the structure, with methylene protons expected in the 1.4−3.4 ppm range, and ammonium ones in the 4.8−11.4 ppm range. These ranges are broadly compatible with the observations; however, the two methylene protons effectively yield two separate signals only in the case of α-glycine, while the ammonium protons always give rise to a single broad signal in experimental spectra. In fact, unless one could work at very low temperatures, the correlation time for proton hopping between the three N−H sites has been reported to be small on the NMR time scale,[86] so that it is not surprising to observe a single averaged signal. It makes sense therefore to compare the experimental proton shift with the average of the three calculated values. In the same way, for β- and γ-glycine, the experimental proton shift in the methylene region will be compared with the average of the two calculated values (however, for α-glycine, the two independent experimental values may be used). This procedure, which has already been used in a previous theoretical simulation of NMR spectra of α-glycine,[88] leaves us with seven independent experimental checks of the chemical shifts calculations for each level of optimization (except for the calculations based on the neutron-diffraction estimates of hydrogen positions since no estimates are available for β-glycine). As can be seen in Figure 4, there is very good agreement between the experimental chemical shifts and the calculated ones, whatever the level of optimization. In fact, the linear correlation coefficient is almost invariant along the optimization steps, with ρ = 0.9978 (H only), 0.9976 (all atoms), 0.9976 (atoms + cell) − only when the neutron diffraction H positions are used is it a little lower (ρ = 0.9958).

Put another way, the standard deviation of the differences between the experimental and calculated values is between 0.2 and 0.25 ppm, which may be considered as an estimate of the precision of the ^{1}H chemical shifts calculations.

5.2. ^{13}C CP-MAS NMR. In line with previously published data, the ^{13}C CP/MAS NMR spectra of the three forms of glycine show peaks in two different regions, around 43 ppm corresponding to the methylene groups, and around 175 ppm,

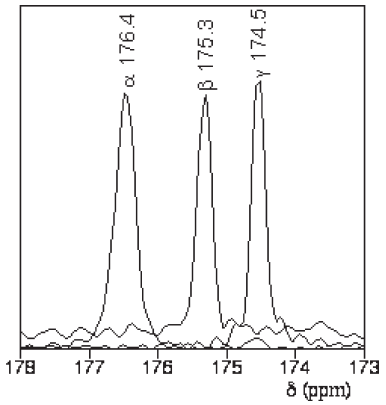

Figure 5. Carboxylate region of the experimental ^{13}C CP-MAS NMR spectra of α-, *β*-, and *γ*-glycine.

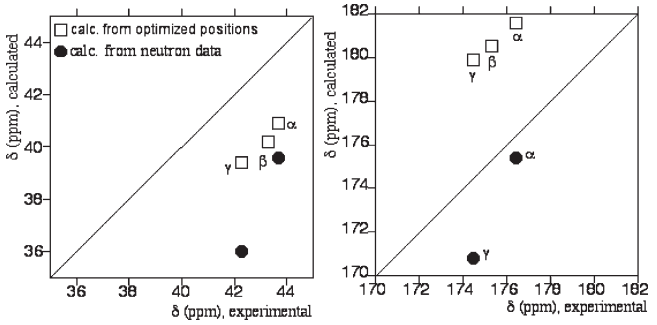

Figure 6. Comparison of calculated and experimental ^{13}C NMR isotropic chemical shifts for the methylene (left) and carboxylate group (right) in α-, *β*-, and *γ*-glycine.

corresponding to the carboxylate groups. The differences in chemical shifts among the three forms of glycine are more marked in the carboxylate region (Figure 5). At room temperature, bulk α-glycine has an isotropic peak at +176.4 ppm (as compared to 176.4 ppm in ref 89), *β*-glycine at +175.3 ppm (175.5 ppm in ref 84), and *γ*-glycine at +174.5 ppm (174.5−174.6 ppm in refs 84 and 89, respectively). Smaller differences, on the order of about 0.5 ppm, are observed between the methylene groups of α-, *β*-, and *γ*-glycine. This is not surprising since the carboxylate groups are more involved than the methylene in the H-bonds networks, which are characteristic of the crystalline form.

The comparison of the experimental chemical shifts with the calculated ones is shown for the two carbon atoms in Figure 6.

If we focus on the carboxylate carbons (right part of figure), the correlation between H-only optimizations and experiment is not very good since the correct order of chemical shifts is not predicted. Allowing all-atoms relaxation provides a much better correlation with the experiment: not only is the correct order predicted, but the chemical shifts differences predicted between the three forms are very much the same as in the experimental spectra, although there is a systematic error of about +5 ppm (i.e., predicted chemical shifts are too high by 5 ppm) contrary to the case of protons where absolute values are correctly predicted. Allowing cell relaxation in addition does not improve the fit.

This difference in absolute value does not seem to be an effect of temperature since the already cited work of Taylor et al.[86] found that the chemical shifts in α-glycine vary by less than one ppm over a range of 200 K.

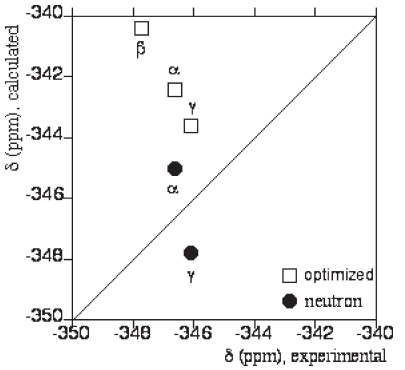

Figure 7. Comparison of calculated and experimental ^{15}N NMR isotropic chemical shifts for the ammonium group in α-, *β*-, and *γ*-glycine.

Similar conclusions may be drawn for the methylene carbons: a good linear correlation with experiment is obtained, but with a systematic error, this time negative, at about −3 ppm. Thus, variations of chemical shifts can be predicted within approximately 0.2 ppm, but absolute values are much less precise.

5.3. ^{15}N CP-MAS NMR. The ^{15}N CP-MAS NMR spectra of the three forms of glycine show the presence of a single peak attributable to the ammonium group of zwitterionic glycine. In spite of the generally high sensitivity of ^{15}N chemical shifts on changes of the chemical environment of the nitrogen atoms, the isotropic chemical shift varies only slightly among the three glycine structures, the three values lying in a range of about 1.5 ppm (−346.6, −347.7, and −346.1 in α-, *β*-, and *γ*-glycine, respectively). These values can be compared to the calculated ones, as shown in Figure 7.

In contrast to ^{1}H and ^{13}C NMR, calculated and experimental ^{15}N chemical shifts are poorly correlated. This bad agreement among these data is measured at each degree of optimization of the structures of glycine. It is difficult to explain these results, but it can be noticed that in the case of ^{15}N, the chemical shift range observed for the various polymorphs is particularly small compared to the global range observed for this nucleus. Moreover, a better agreement between experimental/calculated NMR parameters for ^{1}H and ^{13}C than for ^{15}N using this method has already been observed previously in morpholine- and imidazole-based compounds.[90]

Conclusions

The polymorphs of glycine represent an interesting testing ground to probe the supramolecular arrangements of biological molecules. Several DFT molecular modeling techniques had already been applied to theses compounds; we have extended the range of experimental data against which they can be evaluated by including a characterization through both vibrational spectroscopies (IR in the ATR mode, Raman) and multinuclear solid-state NMR.

While the approach used here (periodic DFT with the rPBE functional) still lacks the precision to correctly predict the small energy differences between the α, *β*, and *γ* polymorphs of glycine, it allows partitioning of the energy of the different structures in a way that shows well-defined units of structural organization: for α-glycine, planar sheets of H-bonded $HGly^{\pm}$ zwitterions, and at a higher level layers that associate two successive sheets; for *β*-glycine, single sheets in an infinite stacking; and for *γ*-glycine, helicoidal columns, also of H-bonded $HGly^{\pm}$ zwitterions, arranged in a honeycomb lattice.

Vibrational frequencies in the 600−1700 cm^{-1} range are predicted within 2−3% by calculations, even without anharmonic corrections. This may be considered as a rather successful agreement between the theory and the experiment, but it remains insufficient to accurately predict the small differences observed in the vibrational spectra of the three polymorphs.

^{1}H NMR chemical shifts are predicted with an accuracy of about 0.2 ppm, taking into account that some signals collapse due to functional groups mobility on the NMR time scale. ^{13}C chemical shifts present systematic errors of a few ppm, but the trends between the different polymorphs are correctly reproduced even though they correspond to very small differences on the order of 1 ppm. For ^{15}N, the precision of the method is not yet good enough to reproduce the experimental trends.

Thus, the most straightforward experimental identification of the three forms of glycine, which is based on the small but very reproducible chemical shift differences between the polymorphs, can now be accounted for on a theoretical basis.

Hopefully, the results discussed here will be used as a standard against which to check further improvements of molecular modeling methodology.

Acknowledgment. The computation facilities are provided by IDRIS, CINES and by CCRE (Université Pierre et Marie Curie − Paris 6). We thank Pr. F. Mauri and Dr. A. P. Seitsonen for the NMR GIPAW module. N.F. benefitted from a Ph.D. grant from the CNano program of the Ile-de-France region. Alessandro Motta from the University of Catania, Italy, is thanked for the calculation of thermodynamics data on the glycine phases with the Dmol3 software.

References

(1) Boldyreva, E. In *Models, Mystery and Magic of Molecules*; Boeyens, J. C. A., Ogilvie, J. F., Eds.; Springer: New York, 2008.
(2) Bernal, J. D. *Z. Kristallogr.* **1933**, *78*, 363.
(3) Bamford, C. H.; Brown, L.; Cant, E. M.; Elliott, A.; Hanby, W. E.; Malcolm, B. R. *Nature* **1955**, *176*, 396.
(4) Kajava, A. V. *Acta Crystallogr. D* **1999**, *55*, 436.
(5) Crick, F. H. C.; Rich, A. *Nature* **1955**, *176*, 780.
(6) Suresh, C. G.; Vijayan, M. *Int. J. Pept. Protein Res.* **1983**, *22*, 129.
(7) McCammon, J. A.; Karplus, M. *Annu. Rev. Phys. Chem.* **1980**, *31*, 29.
(8) Karplus, M.; McCammon, J. A. *Annu. Rev. Biochem.* **1983**, *52*, 263.
(9) Ferrari, E. S.; Davey, R. J.; Cross, W. I.; Gillon, A. L.; Towler, C. S. *Cryst. Growth Des.* **2003**, *3*, 53.
(10) Bordallo, H. N.; Boldyreva, E. V.; Buchsteiner, A.; Koza, M. M.; Landsgesell, S. *J. Phys. Chem. B* **2008**, *112*, 8748.
(11) Harris, R. K. *Analyst* **2006**, *131*, 351.
(12) Bernstein, J. *Polymorphism in Molecular Crystals*; Clarendon Press: Oxford, 2002.
(13) Lee, A. Y.; Lee, I. S.; Dette, S. S.; Boerner, J.; Myerson, A. S. *J. Am. Chem. Soc.* **2005**, *127*, 14982.
(14) Weissbuch, I.; Torbeev, V. Y.; Leiserowitz, L.; Lahav, M. *Angew. Chem., Int. Ed.* **2005**, *44*, 3226.
(15) Poornachary, S. K.; Chow, P. S.; Tan, R. B. H.; Davey, R. J. *Cryst. Growth Des.* **2007**, *7*, 254.
(16) Poornachary, S. K.; Chow, P. S.; Tan, R. B. H. *Cryst. Growth Des.* **2008**, *8*, 179.
(17) Yang, X.; Lu, J.; Wang, X.-J.; Ching, C.-B. *J. Cryst. Growth* **2008**, *310*, 604.
(18) Hughes, C. E.; Harris, K. D. M. *New J. Chem.* **2008**, *33*, 713.
(19) Iitaka, Y. *Acta Crystallogr.* **1960**, *13*, 35.
(20) Iitaka, Y. *Acta Crystallogr.* **1961**, *14*, 1.
(21) Jonsson, P. G.; Kvick, A. *Acta Crystallogr. B* **1972**, *72*, 1827.
(22) Power, L. F.; Turner, K. E.; Moore, F. H. *Acta Crystallogr. B* **1976**, *32*, 11.
(23) Kvick, Å.; Canning, W. M.; Koetzle, T. F.; Williams, G. G. B. *Acta Crystallogr. B* **1980**, *36*, 115.
(24) Drebushchak, T. N.; Boldyreva, E. V.; Seretkin, Y. V.; Shutova, E. S. *Zh. Struktur. Khim.* **2002**, *43*, 899.
(25) Boldyreva, E. V.; Drebushchak, V. A.; Drebushchak, T. N.; Paukov, I. E.; Kovalevskaya, Y. A.; Shutova, E. S. *J. Therm. Anal. Calorim.* **2003**, *73*, 409.
(26) Towler, C.; Davey, R. J.; Lancaster, R. W.; Price, C. J. *J. Am. Chem. Soc.* **2004**, *126*, 13347.
(27) Boldyreva, E. V.; Drebushchak, V. A.; Drebushchak, T. N.; Paukov, I. E.; Kovalevskaya, Y. A.; Shutova, E. S. *J. Therm. Anal. Calorim.* **2003**, *73*, 419.
(28) Drebushchak, V. A.; Boldyreva, E. V.; Drebushchak, T. N.; Shutova, E. S. *J. Cryst. Growth* **2002**, *241*, 266.
(29) Almlof, J.; Kvick, A.; Thomas, J. O. *J. Chem. Phys.* **1973**, *59*, 3901.
(30) Freeman, C. M.; Andzelm, J. W.; Ewig, C. S.; Hill, J. R.; Delley, B. *Chem. Commun.* **1998**, *22*, 2455.
(31) Raabe, G. *Z. Naturforsch.* **2000**, *55*, 609.
(32) Chisholm, J. A.; Motherwell, S.; Tulip, P. R.; Parsons, S.; Clark, S. J. *Cryst. Growth Design* **2005**, *5*, 1437.
(33) Tuma, C.; Boese, A. D.; Handy, N. C. *Phys. Chem. Chem. Phys.* **1999**, *1*, 3939.
(34) Chowdhry, B. Z.; Dines, T. J.; Jabeen, S.; Withnall, R. *J. Phys. Chem. A* **2008**, *112*, 10333.
(35) Day, G. M.; Motherwell, W. D. S.; Jones, W. *Cryst. Growth Des.* **2005**, *5*, 1023.
(36) Rivera, S. A.; Allis, D. G.; Hudson, B. S. *Cryst. Growth Des.* **2008**, *8*, 3905.
(37) Gervais, C.; Dupree, R.; Pike, K. J.; Bonhomme, C.; Profeta, M.; Pickard, C. J.; Mauri, F. *J. Phys. Chem. A* **2005**, *109*, 6960.
(38) Chernobai, G. B.; Chesalov, Y. A.; Burgina, E. B.; Drebushchak, T. N.; Boldyreva, E. V. *J. Struct. Chem.* **2007**, *48*, 332.
(39) Murli, C.; Sharma, S. M.; Karmakar, S.; Sikka, S. K. *Phys. B* **2003**, *339*, 23.
(40) Murli, C.; Thomas, S.; Venkateswaran, S.; Sharma, S. M.; Karmakar, S.; Sikka, S. K. *Phys. B* **2005**, *364*, 233.
(41) Goryainov, S. V.; Boldyreva, E. V.; Kolesnik, E. N. *Chem. Phys. Lett.* **2006**, *419*, 496.
(42) Goryainov, S. V.; Kolesnik, E. N.; Boldyreva, E. V. *Phys. B* **2005**, *357*, 340.
(43) Lesage, A.; Sakellariou, D.; Hediger, S.; Elena, B.; Charmont, P.; Steuernagel, S.; Emsley, L. *J. Magn. Reson.* **2003**, *163*, 105.
(44) Lopes, I.; Piao, L.; Stievano, L.; Lambert, J.-F. *J. Phys. Chem. C* **2009**, *113*, 18163.
(45) Kresse, G.; Furthmüller, J. *Comput. Mater. Sci.* **1996**, *6*, 15.
(46) Perdew, J. P.; Burke, K.; Ernzerhof, M. *Phys. Rev. Lett.* **1997**, *78*, 796.
(47) Tielens, F.; Gervais, C.; Lambert, J.-F.; Mauri, F.; Costa, D. *Chem. Mater.* **2008**, *20*, 3336.
(48) Santra, B.; Michaelides, A.; Scheffler, M. *J. Chem. Phys.* **2007**, *127*, 184104.
(49) Kristyan, S.; Pulay, P. *Chem. Phys. Lett.* **1995**, *229*, 175.
(50) Improta, R.; Barone, V. *J. Comput. Chem.* **2004**, *25*, 1333.
(51) Perez-Jorda, J. M.; Becke, A. D. *Chem. Phys. Lett.* **1995**, *233*, 134.
(52) Kohn, W.; Meir, Y.; Makarov, D. E. *Phys. Rev. Lett.* **1998**, *80*, 4153.
(53) Chocholousova, J.; Vacek, J.; Huisken, F.; Werhahn, O.; Hobza, P. *J. Phys. Chem. A* **2002**, *106*, 11540.
(54) de Carvalho, M. F.; Mosquera, R. A.; Rivelino, R. *Chem. Phys. Lett.* **2007**, *445*, 117.
(55) Tsuzuki, S.; Lüthi, H. P. *J. Chem. Phys.* **2001**, *114*, 3949.
(56) Couronne, O.; Ellinger, Y. *Chem. Phys. Lett.* **1999**, *306*, 71.
(57) Papamokos, G. V.; Demetropoulos, I. *J. Phys. Chem. A* **2004**, *108*.
(58) Tulip, P. R.; Clark, S. J. *Phys. Rev. B* **2005**, *71*, 195117.
(59) Civalleri, B.; Doll, K.; Zicovich-Wilson, C. M. *J. Phys. Chem. B* **2007**, *111*, 26.
(60) Wu, Q.; Yang, W. *J. Chem. Phys.* **2002**, *116*, 515.
(61) Guerra, C. F.; Bickelhaupt, F. M.; Snijders, J. G.; E.J., B. *J. Am. Chem. Soc.* **2000**, *122*, 4117.
(62) Blöchl, P. E. *Phys. Rev. B* **1994**, *50*, 17953.
(63) Kresse, G.; Furthmüller, J. *Phys. Rev. B* **1996**, *54*, 11169.
(64) Lomenech, C.; Bery, G.; Costa, D.; Stievano, L.; Lambert, J.-F. *ChemPhysChem* **2005**, *6*, 1061.
(65) Costa, D.; Tougerti, A.; Tielens, F.; Gervais, C.; Stievano, L.; Lambert, J.-F. *Phys. Chem. Chem. Phys.* **2008**, *10*, 6360.
(66) Giannozzi, P.; Baroni, S.; Bonini, N.; Calandra, M.; Car, R.; Cavazzoni, C.; Ceresoli, D.; Chiarotti, G. L.; Cococcioni, M.; Dabo, I.; Dal Corso, A.; de Gironcoli, S.; Fabris, S.; Fratesi, G.; Gebauer, R.; Gerstmann, U.; Gougoussis, C.; Kokalj, A.; Lazzeri, M.; Martin-Samos, L.; Marzari, N.; Mauri, F.; Mazzarello, R.; Paolini, S.; Pasquarello, A.; Paulatto, L.; Sbraccia, C.; Scandolo,

S.; Sclauzero, G.; Seitsonen, A. P.; Smogunov, A.; Umari, P.; Wentzcovitch, R. M. *J. Phys. Cond. Matt.* **2009**, *21*, 395502.
(67) http://www.quantum-espresso.org/ accessed on March 19, 2010.
(68) Pickard, C. J.; Mauri, F. *Phys. Rev. B* **2001**, *63*, 245101.
(69) Gervais, C.; Coelho, C.; Azais, T.; Maquet, J.; Laurent, G.; Pourpoint, F.; Bonhomme, C.; Florian, P.; Alonso, B.; Guerrero, G.; Mutin, P. H.; Mauri, F. *J. Magn. Reson.* **2007**, *187*, 131.
(70) Dwivedi, A. M.; Krimm, S. *Biopolymers* **1982**, *21*, 2377.
(71) Williams, R. W. *J. Mol. Struct. - Theochem.* **2004**, *685*, 101.
(72) Laulicht, I.; Pinchas, S.; Samuel, D.; Wasserman, I. *J. Phys. Chem.* **1966**, *70*, 2719.
(73) Chakraborty, D.; Manogaran, S. *Chem. Phys. Lett.* **1998**, *194*, 56.
(74) Suzuki, S.; Shimanouchi, T.; Tsuboi, M. *Spectrochim. Acta* **1963**, *19*, 1195.
(75) Machida, K.; Kagayama, A.; Saito, Y.; Kuroda, Y.; Uno, T. *Spectrochim. Acta Part A* **1977**, *33*, 569.
(76) Baran, J.; Ratajczak, H. *Spectrochim. Acta Part A* **2005**, *61*, 1611.
(77) Bielecki, A.; Kolbert, A. C.; Levitt, M. H. *Chem. Phys. Lett.* **1989**, *155*, 341.
(78) Vinogradov, E.; Madhu, P. K.; Vega, S. *Chem. Phys. Lett.* **1999**, *314*, 443.
(79) Sakellariou, D.; Lesage, A.; Hodgkinson, P.; Emsley, L. *Chem. Phys. Lett.* **2000**, *319*, 253.
(80) Madhu, P. K.; Vinogradov, E.; Vega, S. *Chem. Phys. Lett.* **2004**, *394*, 423.
(81) Brus, J.; Petrícková, H.; Dybal, J. *Sol. State Nucl. Mag. Res.* **2003**, *23*, 183.
(82) Coelho, C.; Rocha, J.; Madhu, P. K.; Mafra, L. *J. Magn. Reson.* **2008**, *194*, 264.
(83) Kimura, H.; Nakamura, K.; Eguchia, A.; Sugisawa, H.; Deguchi, K.; Ebisawa, K.; Suzuki, E.-i.; Shojia, A. *J. Mol. Struct.* **1998**, *447*, 247.
(84) Taylor, R. E. *Concepts Magn. Reson.* **2004**, *22A*, 79.
(85) Vinogradov, E.; Madhu, P. K.; Vega, S. *Chem. Phys. Lett.* **2002**, *354*, 193.
(86) Taylor, R. E.; Dybowski, C. *J. Mol. Struct.* **2008**, *889*, 376.
(87) Taylor, R. E.; Chim, N.; Dybowski, C. *J. Mol. Struct.* **2007**, *830*, 147.
(88) Yoon, Y.-G.; Pfrommer, B. G.; Louie, S. G.; Canning, A. *Sol. State Com.* **2004**, *131*, 15.
(89) Potrzebowski, M. J.; Tekely, P.; Dusausay, Y. *Solid State Nucl. Magn. Reson.* **1998**, *11*, 253.
(90) Bouchmella, K.; Dutremez, S. G.; Alonso, B.; Mauri, F.; Gervais, C. *Cryst. Growth Design* **2008**, *8*, 3941.
(91) Yamada, K.; Honda, H.; Yamazaki, T.; Yoshida, M. *Solid State Nucl. Mag. Reson.* **2006**, *30*, 162.